Brain-Penetrating Nanoparticles Improve Paclitaxel Efficacy in Malignant Glioma Following Local Administration

Elizabeth Nance,[†,⊗] Clark Zhang,[†,‡] Ting-Yu Shih,[§,△] Qingguo Xu,[†,∥] Benjamin S. Schuster,[†,‡] and Justin Hanes[*,†,‡,§,∥,⊥,#]

[†]Center for Nanomedicine at the Wilmer Eye Institute, [‡]Department of Biomedical Engineering, [∥]Department of Ophthalmology, [#]Deparments of Oncology, Pharmacology and Molecular Sciences, and Neurosurgery, Johns Hopkins University School of Medicine, Baltimore, Maryland 21231, United States and [§]Department of Chemical & Biomolecular Engineering and [⊥]Center for Cancer Nanotechnology Excellence, Institute for NanoBioTechnology, Johns Hopkins University, Baltimore, Maryland 21218, United States. [⊗]Present address: Department of Anesthesiology and Critical Care Medicine, Johns Hopkins University, Baltimore, Maryland 21218, United States. [△]Present address: School of Engineering and Applied Sciences, Harvard University, Cambridge, Massachusetts 02138, United States.

ABSTRACT Poor drug distribution and short drug half-life within tumors strongly limit efficacy of chemotherapies in most cancers, including primary brain tumors. Local or targeted drug delivery *via* controlled-release polymers is a promising strategy to treat infiltrative brain tumors, which cannot be completely removed surgically. However, drug penetration is limited with conventional local therapies since small-molecule drugs often enter the first cell they encounter and travel only short distances from the site of administration. Nanoparticles that avoid adhesive interactions with the tumor extracellular matrix may improve drug distribution and sustain drug release when applied to the tumor area. We have previously shown model polystyrene nanoparticles up to 114 nm in diameter were able to rapidly diffuse in normal brain tissue, but only if coated with an exceptionally dense layer of poly(ethylene glycol) (PEG) to reduce adhesive interactions. Here, we demonstrate that paclitaxel (PTX)-loaded, poly(lactic-*co*-glycolic acid) (PLGA)-*co*-PEG block copolymer nanoparticles with an average diameter of 70 nm were able to diffuse 100-fold faster than similarly sized PTX-loaded PLGA particles (without PEG coatings). Densely PEGylated PTX-loaded nanoparticles significantly delayed tumor growth following local administration to established brain tumors, as compared to PTX-loaded PLGA nanoparticles or unencapsulated PTX. Delayed tumor growth combined with enhanced distribution of drug-loaded PLGA-PEG nanoparticles to the tumor infiltrative front demonstrates that particle penetration within the brain tumor parenchyma improves therapeutic efficacy. The use of drug-loaded brain-penetrating nanoparticles is a promising approach to achieve sustained and more uniform drug delivery to treat aggressive gliomas and potentially other brain disorders.

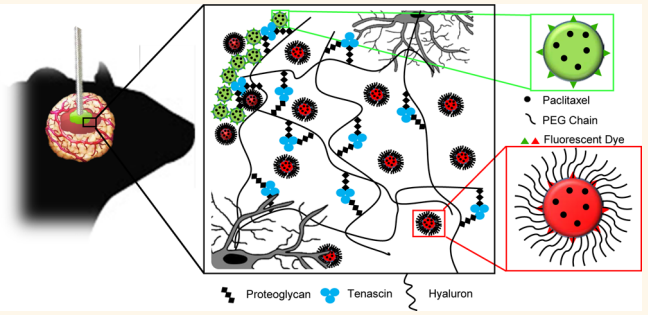

KEYWORDS: nanomedicine · drug delivery · brain cancer · particle tracking

Tissue-specific drug delivery is a critical need for many diseases, including brain cancers, to achieve more effective therapies and reduced side effects. Malignant gliomas (MG) account for 40% of primary brain tumors and result in the loss of more than 15 000 American lives each year.[1,2] Without treatment, most patients live fewer than 3 months; with the most aggressive combination therapies, the median survival is still less than 20 months.[3] The presence of infiltrating tumor cells, which can be found far from the main tumor mass, leads to tumor recurrence in 100% of patients, even after apparent complete surgical resection.[4] The current standard of care for patients with MG consists of surgery, followed by radiation and chemotherapy to treat the residual, infiltrating tumor cells.[5] Strategies to improve current treatments using drug delivery methods have been limited due to the difficulty in achieving a sufficient concentration of chemotherapy at the sites of invasive tumor cells. Limited uptake across the blood brain barrier (BBB) and poor penetration of brain tissue are

* Address correspondence to hanes@jhu.edu.

Received for review July 29, 2014 and accepted September 26, 2014.

Published online September 26, 2014
10.1021/nn504210g

TABLE 1. Characterization of PS, PS-PEG, Paclitaxel (PTX)-loaded PLGA and PLGA-PEG Nanoparticles made in CHA[a]

particle	mean diameter ± SEM (nm)	ζ-potential ± SEM (mV)	PDI	D_{ACSF}/D_{9L}	paclitaxel loading (wt %)
60 nm PS-COOH	55 ± 2.0	−45 ± 1.0	0.09	1500	NA
70 nm PS-PEG5k	74 ± 2.0	−2.5 ± 0.1	0.10	130[b]	NA
90 nm PS-COOH	89 ± 1.0	−55 ± 3.0	0.07	>10 000	NA
100 nm PS-PEG5k	102 ± 3.0	−4.4 ± 0.2	0.08	500[b]	NA
220 nm PS-COOH	223 ± 1.0	−47 ± 2.2	0.11	>10 000	NA
240 nm PS-PEG5k	237 ± 4.0	−5.4 ± 0.2	0.10	9700	NA
PLGA	88 ± 4	−48 ± 4	0.15	>10 000	5.3 ± 1.0
PLGA-PEG	69 ± 4	−2.2 ± 0.2	0.11	99[b]	4.9 ± 1.1

[a] Mean diameter in ACSF at pH 7.0 was measured using dynamic light scattering. ζ-Potential and PDI were measured in ACSF at pH 7.0. Effective diffusivity values in excised intracranial 9L gliosarcoma (D_{9L}) are calculated at a time scale of 1 s. D_{ACSF} is calculated from the Stokes−Einstein equation. Paclitaxel loading was quantified by HPLC. [b] $p < 0.05$ compared to PLGA (ANOVA).

considerable obstacles to improving drug efficacy against infiltrative malignant tumor cells.[6,7]

Local chemotherapy, provided by either biodegradable polymer implants[8] or convection-enhanced delivery,[9−12] has been utilized to bypass the BBB and provide sustained drug release, leading to improved toxicity profiles and reduced dosing frequency.[13,14] Drug-loaded polymeric nanoparticles formulated with surfactant coatings, such as polysorbate 80 and poloxamer 107, allow transport across the BBB[15] and have shown efficacy against rat glioblastomas.[16−18] These particles increase therapeutic uptake into the brain, but appear to move from endothelial cells to neurons close to the BBB *via* a cell-to-cell process, thereby not addressing the penetration barrier within the brain tumor parenchyma. Nanoparticles able to overcome this barrier may achieve improved distribution within the brain, potentially leading to improved drug delivery and efficacy against various diseases, including MG.

To address this challenge, we developed nanoparticles capable of rapid diffusion within the brain parenchyma ("brain-penetrating nanoparticles", or BPNs) by coating nanoparticles with a dense layer of low MW poly(ethylene glycol) (PEG), a hydrophilic and uncharged polymer, which effectively minimizes adhesive interactions between the particle and charged or hydrophobic components within the brain parenchyma.[19] Here, we first used these model BPNs to determine nanoparticle diffusion as a function of size and surface functionality in rat 9L gliosarcoma brain tumors. On the basis of our findings, we next developed a biodegradable polymeric nanoparticle platform and tested whether drug-loaded nanoparticles capable of rapid penetration within intracranial 9L glioma improve efficacy of a chemotherapeutic agent, as compared to otherwise similar nanoparticles that lack the ability to penetrate efficiently and as compared to unencapsulated drug.

RESULTS AND DISCUSSION

Model Brain-Penetrating Nanoparticle Diffusion in Gliomas. Whether nanoparticles reach brain tumors by the enhanced permeation and retention (EPR) effect or by direct administration during or after surgery, they must be able to penetrate within the brain microenvironment to reach infiltrative cells that cause tumor recurrence and to provide more uniform drug distribution within tumors. We first engineered nanoparticles with exceptionally dense PEG coatings (above 9 PEG/100 nm^2; Table 1), which we previously showed could penetrate brain tissue of healthy mice, rats, and humans.[19] To determine the effect of the tumor microenvironment on the ability of nanoparticles to diffuse within the tumor parenchyma, fluorescent polystyrene (PS) particles with carboxyl (COOH) or dense PEG coatings (Table 1) were added to freshly excised 9L gliosarcoma tissue. Individual particle movements within 9L gliomas from rats were quantified using high-resolution multiple particle tracking (MPT). PEG-coated particles used were 10−20 nm larger than the COOH-coated particles and had a near-neutral net surface charge (Table 1). The 70 nm PEG-coated nanoparticles penetrated 9L tumor tissue with an average effective diffusivity that was 12-fold higher than similarly sized COOH-coated particles (Figure 1A; Table 1). Standard COOH-coated PS particles (PS-COOH) diffused 1500 times slower in 9L tumors compared to in artificial cerebrospinal fluid (ACSF) (Table 1). On the other hand, the 70 nm PS-PEG particles diffused only 130-fold slower in 9L gliosarcomas compared to theoretical diffusivities of same-sized particles in ACSF and 14-fold slower than the same PS-PEG particles in normal rat brain tissue (Figure 1A).

As we have previously shown in normal tissue, rapid transport of 70 and 100 nm PS-PEG particles in brain tissue is expected only if a substantial number of spacings within the brain extracellular space (ECS) microenvironment are greater than 100 nm.[19] However, in 9L gliosarcomas, 100 nm PS-PEG particles had 8-fold slower diffusion compared to 100 nm PS-PEG particles in normal rat brain tissue (Figure 1A). PEG-coated particles of 240 nm diffused approximately 19-fold slower than the 100 nm PEG-coated particles in the tumor (Figure 1A). Representative particle trajectories for both PEG-coated and COOH-coated particles

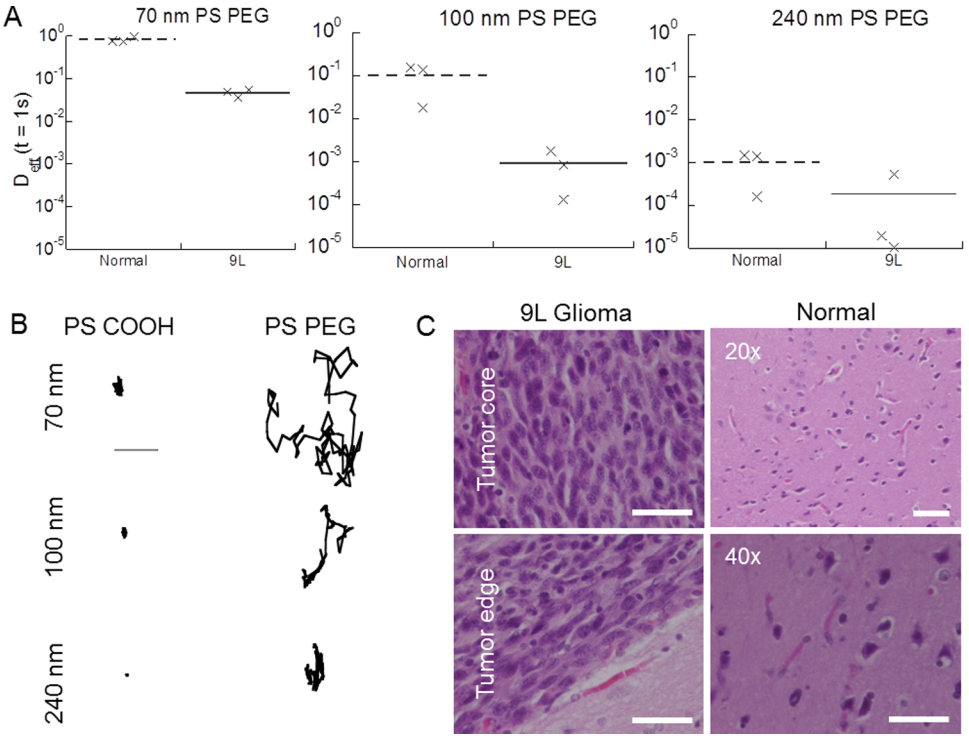

Figure 1. Multiple particle tracking analysis of model nanoparticles in 9L gliosarcoma. (A) Ensemble-averaged effective diffusivities (D_{eff}, $\mu m^2/s$) at 1 s for 70, 100, and 240 nm PS-PEG NPs in normal rat brain and 9L gliosarcoma tissue for $N = 3$ rats per particle size. Lines indicate average D_{eff} at $t = 1$ s for $N = 3$ samples. Data represent means of at least three samples, with $n >$ 500 particles per particle type and sample. (B) Representative particle trajectories for COOH- and PEG-coated NPs of various sizes in freshly excised 9L gliosarcomas. Trajectories shown are of particles tracked over an equivalent number of frames, which possessed a mean-squared displacements (MSD) within one standard deviation of the ensemble average at a time scale of 1 s (scale bar 1 μm). (C) Histological analysis of tumor cellularity and ECS at the tumor core and tumor edge of 9L sarcomas and magnified images of comparable normal tissue where nanoparticles were tracked. Scale bars: 50 μm.

at all sizes studied in brain tumor tissue are provided in Figure 1B, where particles densely coated with PEG exhibited diffusive motion for 70 nm particles, but increasingly hindered motion for 100 and 240 nm particles.

Brain tumors possess substantially higher cell density and greater collagen content than normal brain tissue.[20] Histological analysis in regions where the particles were tracked demonstrates increased tumor cellularity and decreased ECS spacing in 9L tumors compared to normal tissue (Figure 1C). These factors can increase the tortuosity and steric hindrance a particle encounters as the particle size becomes comparable to dimensions of the channels through which they move.[21] In previous studies, the immobilization of COOH-coated polystyrene particles in healthy brain was suggested to be due to exposure of the hydrophobic particle core to hydrophobic regions found within normal brain ECS, such as proteoglycans and glycosaminoglycans, including hyaluronan.[22] In tumors, the distribution of ECM components is varied throughout the tumor mass, and it is thought these molecules play a role in tumor cell migration and invasiveness.[20,21,23,24] An increase in ECM components in the tumor would most likely hinder nanoparticle diffusion within the tumor microenvironment, as seen by the hindered or immobilized transport of model PS-PEG greater than 100 nm. While 100 nm PS-PEG NP transport is hindered, suggesting the average spacing in tumors is smaller than in normal tissue, the diffusion of PS-PEG NPs smaller than 100 nm suggests the effective spacing in the ECS is still large enough for effective penetration and distribution of a larger (~70−80 nm) particle.

Physicochemical Characterization of PTX-Loaded Nanoparticles and Release of Drug *in Vitro*. Based on the limited diffusive capabilities of PEG-coated nanoparticles larger than 100 nm in tumor tissue compared to normal brain tissue, we developed sub-100 nm PTX-loaded nanoparticles composed of PLGA-PEG emulsified in a low percent of cholic acid (CHA) (PTX/PLGA-PEG NPs). The narrow size distribution of both PTX/PLGA-PEG NPs and the corresponding conventional PLGA particles without PEG (PTX/PLGA NPs) was confirmed by dynamic light scattering, with average diameters of 69 and 88 nm, respectively (Table 1). The surface charge (ζ-potential) of PTX/PLGA-PEG NPs was approximately −2 mV, consistent with the near-neutral surface charge required for penetration of brain tissue previously reported by our group.[19] The near-neutral surface charge suggests that formulation in CHA and the high weight percent of PEG was sufficient to effectively shield the hydrophobic PLGA core. The drug loading

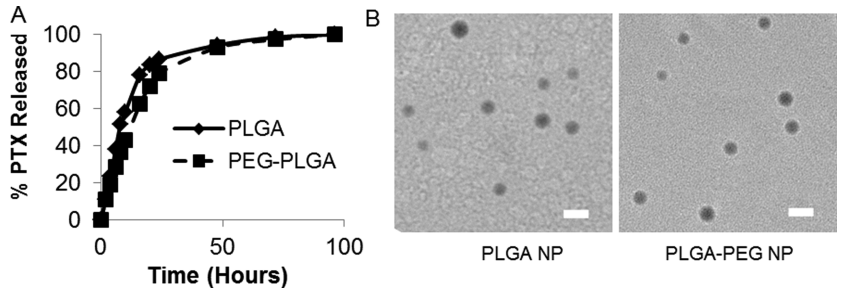

Figure 2. Characterization of PTX-loaded biodegradable nanoparticles. (A) Paclitaxel release kinetics from PLGA NPs and PEG-PLGA NPs made in 0.5% CHA. (B) TEM images of PLGA NPs and PLGA-PEG NPs made in 0.5% CHA showing similar size distributions. Scale bar: 100 nm.

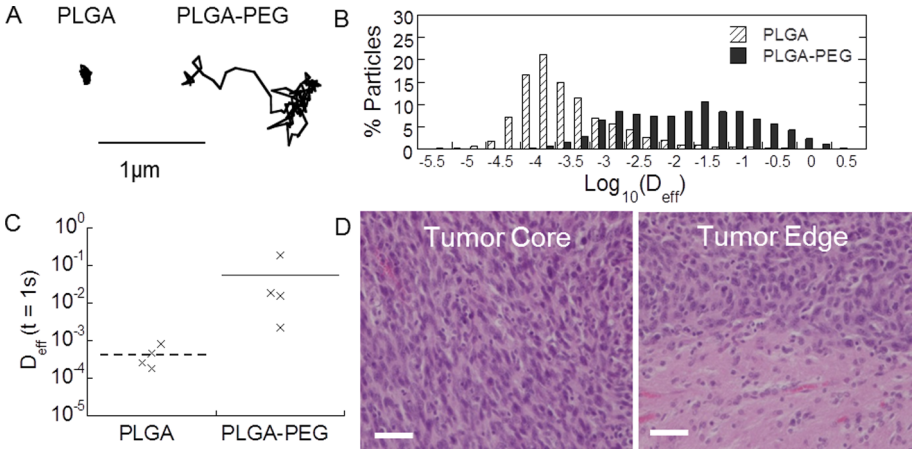

Figure 3. Diffusion of paclitaxel-loaded nanoparticles in intracranial 9L gliosarcoma. (A) Representative particle trajectories for PLGA NPs and PLGA-PEG PTX NPs in the brain tumor microenvironment up to 20 s. (B) Distribution of D_{eff} of individual PTX/PLGA NPs and PTX/PLGA-PEG NPs in excised 9L gliosarcomas. Data represent at least four samples, with $n > 500$ particles per sample, with each sample equally weighted. (C) Effective diffusivities at $t = 1$ s for PTX/PLGA NPs and PTX/PLGA-PEG NPs. The solid lines represent the average D_{eff} ($\mu m^2/s$) at $t = 1$ s for $n = 4$ samples. (D) Representative histological sections from *ex vivo* MPT analysis where particle diffusion was measured at the tumor center (left) and at a well-defined tumor edge (right), showing increased cellularity and decreased ECS compared to normal tissue. Scale bar: 50 μm.

of PTX/PLGA-PEG NPs (4.9% w/w) was comparable to that of PTX/PLGA NPs (5.3%) (Table 1). Both PLGA-PEG NPs and PLGA NPs released PTX over 3 days (Figure 2A), with nearly identical release kinetics. Representative TEM images of both PLGA NPs and PLGA-PEG NPs show narrow size distribution of both particle types (Figure 2B).

PTX-Loaded Nanoparticle Diffusion within *ex Vivo* Glioma Tissue. We next measured PTX/PLGA-PEG NP and PTX/PLGA NP diffusion rates in excised 9L gliosarcomas using MPT. PTX/PLGA NPs were slowed on average 11 000-fold in 9L gliosarcomas compared to their theoretical speeds in ACSF, whereas PTX/PLGA-PEG NPs were slowed only ~100-fold in glioma tissue compared to in ACSF (Table 1). We found PTX/PLGA-PEG NPs, roughly 70 nm in size, penetrated within 9L gliosarcomas (Figure 3A) at rates similar to 70 nm PS-PEG NPs in glioma tissue. The distributions of the logarithms of individual particle effective diffusivities (D_{eff}) showed a near-uniform increase in individual particle speeds for PTX/PLGA-PEG NPs compared to PTX/PLGA NPs (Figure 3B). PTX/PLGA-PEG NPs were 110-fold faster at a time scale of 1 s compared to PTX/PLGA NPs in 9L gliosarcomas (Figure 3C).

Our results suggest the incorporation of PTX during particle formulation did not interfere with PEG partitioning to the surface to effectively shield the PLGA core, allowing the drug-loaded PLGA-PEG nanoparticles to penetrate within freshly excised brain tumor tissue. Representative H & E stained brain slices following MPT demonstrate the tumor microenvironment where nanoparticle diffusion was measured remained intact, including regions of intact tumor tissue and dense cellularity (Figure 3D).

PTX-Loaded Nanoparticle Distribution within 9L Gliomas *in Vivo*. Following surgical resection and/or radiation therapy of brain tumors, chemotherapy is often used to treat residual infiltrative cells in the brain. However, accumulation of systemically administered drug in the brain is minimal due to the BBB,[25,26] limiting the effectiveness of the treatment and increasing adverse side effects. Given that almost all patients with MG undergo tumor resection during which adjuvant therapies may be applied, local delivery of therapeutic

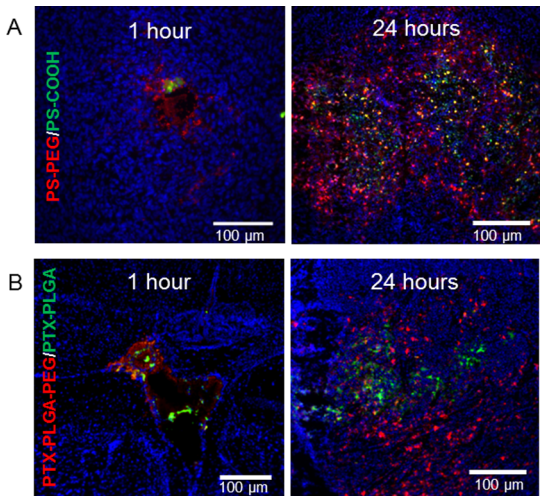

Figure 4. Nanoparticle distribution in intracranial 9L gliosarcomas. (A) PS-PEG NP (red) and PS-COOH NP (green) distribution at 1 and 24 h after direct injection intracranially into the tumor core. Nuclei are stained with DAPI antifade. (B) Distribution of PTX/PLGA NPs (green) and PTX/PLGA-PEG NPs (red) in an intracranial 9L gliosarcoma following intratumoral administration of nanoparticles at 1 h postinjection and 24 h postinjection. Scale bar: 100 μm.

agents in the brain is attractive.[27] We administered fluorescently labeled model PS-PEG NPs, and biodegradable PLGA-PEG NPs or PLGA NPs, intratumorally to rats bearing 9L gliosarcomas and harvested the entire brain at 1 and 24 h after injection. We confirmed that 70 nm PS-PEG NPs, which showed the highest D_{eff} in excised 9L gliosarcoma tissue by MPT, were able to spread within 9L tumors following intratumoral injection *in vivo* (Figure 4). On the other hand, fluorescent images of coronal sections of brain tumor tissue show that PS-COOH NPs (green) remain localized to the pocket of injection, failing to penetrate within the brain parenchyma, and reach the outer tumor edge at 1 h postadministration (Figure 4A). PS-PEG NPs (red) distributed more uniformly throughout the tumor parenchyma over time and away from the injection site. Similarly, we found that biodegradable PTX-loaded PLGA-PEG NPs (red) displayed improved distribution following local administration compared to PTX-loaded PLGA NPs (green) in 9L gliosarcomas (Figure 4B).

These results are important since, as tumor size increases over time, the ability of drugs to penetrate into the tumor decreases due to increased interstitial pressure, increased cellularity, and ECM composition.[28,29] It has been shown that chemotherapeutic drugs achieve limited penetration of solid tumors, due to radial flow of interstitial fluid toward the edge of the tumor and rapid absorption of drug by angiogenic blood vessels.[28,30,31] Although the drugs may kill superficial layers of tumor cells, their inability to fully penetrate into and distribute throughout the tumor parenchyma prevents complete eradication of the tumor.

Strategies that enable sustained and localized chemotherapy delivery in the brain may reduce adverse side effects commonly associated with systemic chemotherapy, while improving efficacy by providing higher drug concentrations at the tumor site and tumor infiltrative front for prolonged periods of time. These images provide evidence that densely PEGylated NPs sub-100 nm in diameter were able to more readily penetrate within the tumor microenvironment compared to non-PEGylated NPs. Furthermore, they remain in the tumor tissue, where they may provide sustained release of PTX to surrounding tumor cells.

PTX-Loaded BPNs Improve Efficacy against 9L Gliosarcomas. We next evaluated the therapeutic efficacy of locally administered PTX/PLGA-PEG NPs ("BPNs") compared to PTX/PLGA NPs or unencapsulated PTX in an intracranial 9L gliosarcoma model. 9L cells genetically modified to express the luciferase enzyme were inoculated intracranially 4 days prior to local administration of Taxol (clinical formulation of PTX), PTX/PLGA NPs, or PTX/PLGA-PEG NPs at 2.5 mg/kg of PTX. Tumors in animals in the control group (no treatment) grew rapidly (Figure 5). By day 15, the tumor load in this group, as reflected by bioluminescence measurements, was 93-fold higher than at day 2. The tumor growth rate in animals that received locally administered Taxol was slightly slower than that of the nontreated control group, with an overall tumor load equal to 85% of the control group by day 15. The average bioluminescence signal for the PTX/PLGA NP group at day 15 was 45% of the nontreated group, indicating improved efficacy compared to local Taxol. However, the tumor load of the PTX/PLGA-PEG NP group was only 8% of the control group and statistically lower than that of any other group ($p < 0.05$) at day 15 (Figure 5).

BPNs markedly enhanced the delivery of PTX in 9L gliosarcoma tissue following a single intratumoral administration, leading to prolonged suppression of growth of an aggressive tumor model. PTX, a frontline chemotherapeutic for the treatment of many cancers, inhibits the growth of tumor cells by stabilizing microtubules and inducing apoptosis of tumor cells.[32] However, penetration of free drugs, like PTX, to cells that have migrated away from the site of tumor resection,[8] thus limiting the applicability of PTX loaded wafer or gel systems for infiltrative tumors. The enhanced efficacy of PTX/PLGA-PEG NPs can be attributed to their ability to penetrate within the brain tumor parenchyma, which facilitates improved particle and drug distribution to a greater proportion of the tumor mass. Uniform distribution allows BPNs to provide an elevated and sustained level of PTX to a larger area of tumor, more effectively suppressing tumor growth. This is in sharp contrast to free PTX administered intratumorally in the form of Taxol, which is more toxic. Unlike PTX/PLGA-PEG NPs, PTX/PLGA NPs did not delay tumor growth compared to Taxol, even though PTX/PLGA NPs exhibited similar size, drug loading, and drug release profiles when compared to PTX/PLGA-PEG NPs.

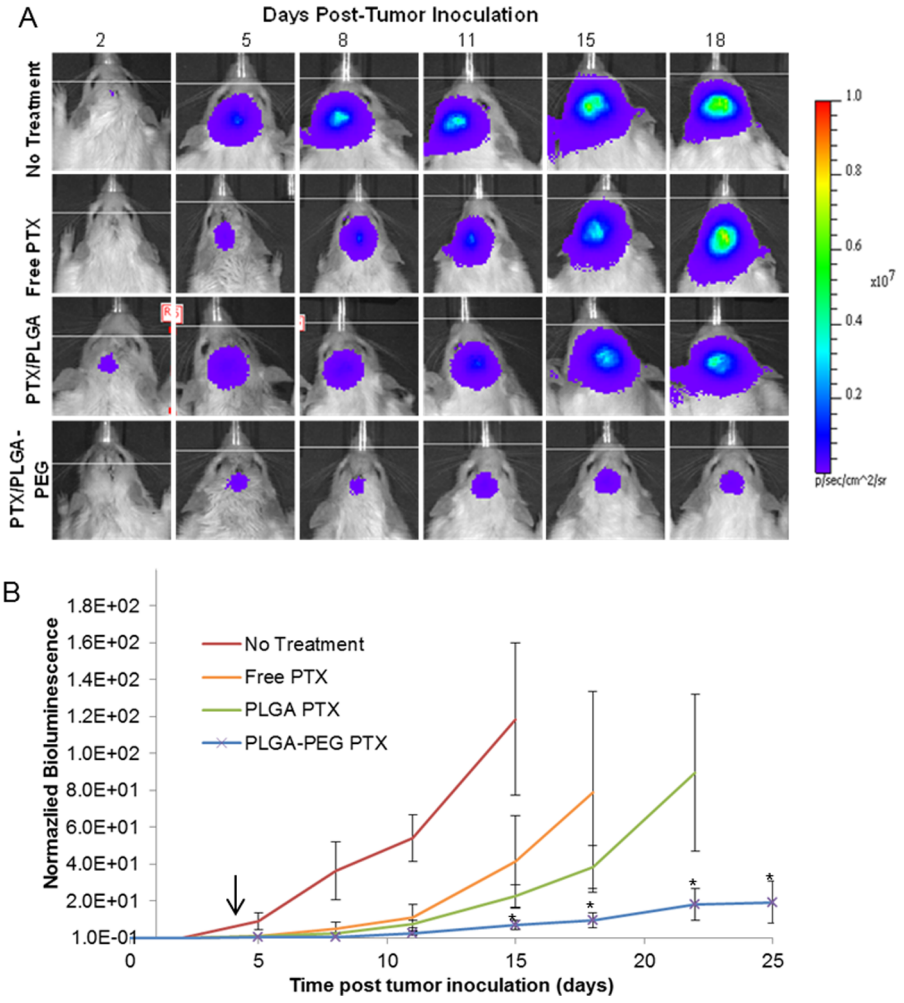

Figure 5. *In vivo* **efficacy in 9L gliosarcoma model in rats. (A) Bioluminescent signal change correlating to tumor growth over time following inoculation. Treatments were administered 4 days following tumor inoculation (indicated by black arrow). (B) Luciferase-expressing 9L gliosarcoma cells (9LL) were intracranially (IC) implanted at 10^4 cells per rat. For the three treatment groups, treatments were given IC on day 4 after inoculation (indicated by black arrow). PTX dosage for all treatment groups was 0.4 mg per rat. Free PTX was administered in a 1:1 solution of 100% ethanol to Cremaphor. PLGA NPs and PLGA-PEG NPs loaded with PTX were administered in normal saline. All rats received 20 μL of the respective treatment. $N = 6$ rats per group. * denotes statistically significant differences ($p < 0.05$, ANOVA) for PTX/PLGA-PEG compared to all other groups.**

Therefore, the lower efficacy of PTX/PLGA NPs against 9L gliosarcomas was likely due to their inability to penetrate within the tumor parenchyma.

Recently, a promising study using convection enhanced delivery of poly(vinyl alcohol) (PVA)-coated PLGA nanoparticles in rodents showed improved distribution and efficacy of a therapeutic against an aggressive glioma.[33] While the effect of the PVA surfactant on the ability of NPs to diffuse within the brain tumor microenvironment has not been investigated, both this study and our current study demonstrate the importance of greater NP distribution following local delivery for improved efficacy against gliomas. In the future, it would be ideal if the brain-penetrating nanoparticles could be administered systemically, thereby allowing repeatable, noninvasive administration of therapeutics, while potentially minimizing side effects and toxicity to normal tissue. Surfactant-coated nanoparticles have been shown to accumulate in the brain parenchyma following systemic administration and improve efficacy of chemotherapeutic agents against MGs[34,35] by delivering therapeutically effective concentrations into the brain. While these particles are able to reach the brain in higher amounts compared to free drug, because they avoid rapid clearance and cross an intact BBB, they internalize in cells and traffic from the BBB by an active cell-to-cell process,[36,37] which may limit their penetration deep into the tumor parenchyma. If delivered systemically, PTX/PLGA-PEG NPs can circulate longer compared to PTX/PLGA NPs due to the PEG coating,[38] providing greater opportunity for PTX/PLGA-PEG NPs to accumulate in the tumor *via* the EPR effect.[39,40] However, the breakdown of the BBB in many tumors is heterogeneous, and therefore particles will still need to cross an intact BBB to reach many parts of the tumor.[41] Magnetic resonance-guided focused ultrasound (MRgFUS) is one promising approach to overcome BBB heterogeneity in tumors.[42−44] We have

recently shown that densely PEG-coated PS and PLGA NPs can accumulate in the brain following systemic administration, when combined with MRgFUS and microbubbles.[45] Although it remains speculative, it is possible that PEG-coated nanoparticles delivered to the brain from the systemic circulation in this manner may be able to penetrate the tumor microenvironment to more evenly distribute a therapeutic payload, potentially leading to improved efficacy.

CONCLUSION

We previously developed model PEG-coated NPs and found that nanoparticles that are much larger than previously expected can rapidly penetrate within normal brain parenchyma, but only if the NPs were densely coated with PEG.[19] Here, we found that 70 nm biodegradable nanoparticles with dense PEG coatings (BPNs) can (1) rapidly diffuse within the brain tumor microenvironment and (2) distribute more evenly throughout the tumor compared to uncoated PLGA nanoparticles and (3) that greater distribution of PTX-loaded BPN leads to improved tumor growth suppression compared to PTX delivered by otherwise similar, but nonpenetrating, NPs and PTX formulated in Cremophor (Taxol). We expect that biodegradable BPNs can be adapted to deliver a variety of therapeutics in the brain and in other tissues and may achieve improved distribution and efficacy compared to conventional particles in other tumors as well as MG. Biodegradable BPNs may find use in treating other aggressive and infiltrative brain diseases and can likely be combined with convection-enhanced delivery for local administration or focused ultrasound[45−48] for delivery to select sites in the CNS following systemic administration.

MATERIALS AND METHODS

Nanoparticle Preparation and Characterization. Forty to 200 nm red fluorescent COOH-modified polystyrene particles (Molecular Probes) were covalently modified with methoxy (MeO)-PEG-amine (NH_2) (5 kDa MW; Creative PEG Works) by carboxyl amine reaction, following a previously described protocol.[19] Briefly, 100 μL of PS particle suspension was washed and resuspended to 4-fold dilution in ultrapure (UP) water. An excess of MeO-PEG-NH_2 was added to the particle suspension and mixed to dissolve the PEG. *N*-Hydroxysulfosuccinimide (Sigma) was added to a final concentration of 7 mM, and 200 mM borate buffer, pH 8.2, was added to a 4-fold dilution of the starting volume. 1-Ethyl-3-(3-(dimethylamino)propyl)carbodiimide (Invitrogen) was added to a concentration of 10 mM. Particle suspensions were placed on a rotary incubator for 4 h at 25 °C and then centrifuged (Amicon Ultra 0.5 mL 100k MWCO; Millipore). Particles were resuspended in ultrapure water to the initial particle volume (100 μL) and stored at 4 °C until use.

PLGA (75:25) polymer (MW: 15 kDa; Jinan Daigang Biomaterials Co. Ltd., Jinan, China), PLGA-PEG (75:25) (25% PEG), and PLGA-PEG (50:50) (10% PEG) copolymers (total MW: 20 and 50 kDa, respectively; Jinan Daigang Biomaterials Co. Ltd., Jinan, China) were labeled with AlexaFluor 555 cadaverine (AF 555, Molecular Probes) fluorescent dye, as described previously.[49] Briefly, the polymers were first dissolved in dichloromethane (DCM) and were activated by *p*-nitrophenyl chloroformate and pyridine. The reaction was carried out for 3 h under constant stirring. The activated polymers were precipitated in 4 °C ethylene ether and were dried overnight under vacuum. Then, the activated polymers and the AF 555 dye were dissolved in dimethylformamide, and triethylamine was added immediately to the polymer−dye mixture. The reaction was carried out for 4 h under constant stirring. The fluorescently labeled polymers were precipitated in 4 °C ethylene ether two to three times and were dried overnight under vacuum.

On the day of intratumoral administration, fluorescently labeled PLGA-PEG and PLGA polymers were dissolved in 1 mL of DCM at 20 and 100 mg/mL, respectively. The polymer solution was added to 5 mL of surfactant solutions (0.5% CHA) immediately followed by sonication (30% magnitude for 2 min) in an ice water bath.[50] Then, the emulsified solution was immediately added to 25 mL of surfactant solutions and was stirred for 3 h to remove solvent while nanoparticle formed simultaneously. The sample solutions were passed through a 1.0 um filter (Whatman), and collected. PLGA-PEG NPs were collected by using centrifugal filtering units (MWCO: 100 kDa, Millipore Ltd. Ireland) at 3600*g* for 12−16 min so that the final sample volume in the filter unit was less than 1 mL. PLGA-PEG NPs were washed three times in UP water. All PLGA NPs were collected by high-speed centrifugation at 22170*g* for 30 min, washed once, and resuspended in normal saline.

9L Gliosarcoma Cell Culture. 9L gliosarcoma cells were provided by Dr. Henry Brem. Briefly, 9L cells were cultured in Dulbecco's modified Eagle's medium supplemented with 1% pen/strep and 10% heat-inactivated fetal bovine serum. To facilitate imaging and tracking of tumor growth, 9L cells were transduced with lentivirus (9L-luc, provided by Dr. Gilson Baia) encoding a constitutively expressing luciferase gene. The luciferase activity was measured using a luciferase reporter assay system.

Intracranial 9L Gliosarcomas and Treatment. All animal experiments were carried out at Johns Hopkins University School of Medicine following National Institutes of Health guidelines and local Institutional Animal Care and Use Committee regulations. A total of 10^4 9L-luc cells in 10 μL of PBS were injected over 10 min into the left striatum of 6−8-week-old female Fischer F344 rats (Harlan). Briefly, 100 mg/mL ketamine and 10 mg/mL xylazine were added to a mixture of 0.9% normal saline and ethanol at a 10:1 ratio. Rats were given 250 μL of ketamine/xylazine solution intraperitoneally (ip). The animals were placed on a stereotaxic head frame, and a burr hole was made 2 mm left of the bregma and 3 mm behind the coronal suture using a 14 mm drill bit. The cell suspension was injected 2.5 mm deep into the brain using a Hamilton syringe (Hamilton, Reno, NV, USA). The incision was sewn with a single double-surgeon's knot using 5−0 Polysorb sutures, and bacitracin was placed on the head wound daily until the wound healed. Animals were monitored daily for neurological changes, and tumor growth was tracked two times a week using the Xenogen IVIS Spectrum optical imaging device and Living Image software (Caliper Life Sciences, Hopkinton, MA, USA), starting at day 2 following tumor inoculation to obtain a baseline luminescent reading.

Rats were given treatments 3 days after tumor inoculation (day 4). Prior to treatment, rats were anesthetized as described above, and the previous incision was cut open to administer treatments intracranially through the same burr hole. Bone regrowth was minimal, but in cases where the bone obscured the original hole a 14 mm drill bit was used to redefine the edges. Rats were placed on the stereotaxic head frame and were administered with PTX/PLGA NPs, PTX/PLGA-PEG NPs (BPNs), or PTX in a 1:1 Cremophor/ethanol solution at a dose of 2.5 mg/kg. Rats with no treatment served as a negative control and were given the same surgical treatment and a saline injection to account for any neurotoxicity or side effects due to the surgical process. Tumor growth was monitored by live bioluminescence imaging with the Xenogen IVIS Spectrum optical imaging device (Caliper Life Sciences) at different time points. The bioluminescence

signals were analyzed by using the Living Image Software (Caliper Life Sciences). Animal weight was taken daily. Animals were monitored daily for neurological changes and sacrificed at the first signs of severe neurological symptoms, including hemiparesis, loss of balance, or hunched behavior.

Brain Tumor Slice Preparation. All experiments were carried out at Johns Hopkins University School of Medicine in accordance with National Institutes of Health guidelines and local Institutional Animal Care and Use Committee regulations. Brain tumor slices were prepared from 160 g female Fischer F344 rats sacrificed 2 weeks following initial 9L-luc tumor inoculation. Animals were anesthetized with ketamine/xylazine and then administered an intracardiac injection of Euthanosol. The whole brain was removed and immersed in chilled ACSF (Harvard Apparatus) supplemented with 10 mM glucose. Coronal slices (n = 6 per animal) were prepared using a rodent brain slice matrix kit (Zivic Instruments). The matrix and razor blades were washed with 0.9% normal saline and placed on ice prior to inserting the excised rodent brain sample. Sectioning of the brain was carried out based on instrument instructions such that 0.5 mm thick slices were obtained. Slices were cut down the midline, and individual sections from the right hemisphere consisting of mostly visibly apparent tumor were placed in a custom-made chamber with a 50 μL well.

Multiple-Particle Tracking in Brain Tumor Slices. Transport of nanoparticles in brain slices was studied by multiple-particle tracking, as we have previously described,[19] and adapted here for brain tumor slices. Briefly, 0.2 μL of PLGA or PLGA-PEG NPs (containing AF555-labeled polymers) was added to 0.5 mm tumor tissue slice samples in custom-made chambers. A glass coverslip was fixed on top with Super Glue to seal the chamber. Samples were then allowed to equilibrate for 10 min at room temperature before imaging. Particles were imaged with a Zeiss Axio Observer D1 epifluorescent microscope (Zeiss). Movies were captured using a 100×/1.46 NA objective on a Photometrics Evolve 512 EMCCD camera (Photometrics) and Metamorph software (Universal Imaging) at a frame rate of 15 Hz for 20 s, as we have previously described.[51] Trajectories of individual particle centroids were obtained with an automated tracking algorithm originally from Crocker and Grier,[52] translated into Matlab code by Blair and Dufresne, and further adapted by our group for nanomedicine applications.[53] Only data from particles tracked for at least 15 frames were included in the analysis. With the particle trajectories obtained from automated tracking analysis, data were analyzed as we have previously described.[19] Briefly, the coordinates of individual nanoparticle centroids were used to calculate time-averaged mean-squared displacements from which diffusivities were calculated. At least 500 particles were tracked per sample, with n = 4 samples per particle condition for PLGA and PLGA-PEG NP studies. Additional information on measuring 3D particle transport by 2D particle tracking is provided in a review article from our group.[54]

Drug Loading. PTX-loaded PLGA and PLGA-PEG NPs were prepared using 15% (w/w) PTX and collected as described above. PTX (15% w/w) was used. To quantify PTX loading, PTX-loaded NPs were lyophilized and dissolved in ACN to extract PTX. Samples were filtered through a 0.2 μm PTFE filter, and then 50 μL of the filtrate was injected into a Shimadzu high-performance liquid chromatography (HPLC) equipped with a C_{18} reverse phase column (5 μm, 4.6 × 250 mm; Varian Inc., Santa Clara, CA, USA). PTX was eluted using an isocratic mobile phase containing 65% acetonitrile in water at 1 mL/min and detected at 230 nm wavelength by a UV detector. The data were analyzed using LC solution software (Shimadzu Scientific Instruments). Drug loading was defined as the ratio of weight of PTX to total weight (polymer plus TX).

$$\text{Drug loading} = \frac{\text{Weight of PTX}}{\text{Total weight of sample(polymer} + \text{PTX)}} \times 100\%$$

***In Vitro* Drug Release.** PTX-loaded PLGA and PLGA-PEG NPs were resuspended in ACSF. Each sample was split into three dialysis tubing cellulose membranes (MWCO: 10 kDa, Spectrum Laboratories, Inc.) (N = 3). Membranes were submerged in 20 mL of ACSF with 0.2% (v/v) P80[55] and were incubated on a shaker at 150 rpm at 37 °C. At designated time points, the membranes were transferred to fresh ACSF with 0.2% P80. Four milliliters of sample collected at each time point was lyophilized. Drug content was determined by HPLC as described above. Percent PTX released was defined as the PTX amount released at a specific time point divided by the total encapsulated PTX.

***In Vivo* Spread of BPN in 9L Gliosarcomas.** All animal experiments were carried out at Johns Hopkins University School of Medicine following National Institutes of Health guidelines and local Institutional Animal Care and Use Committee regulations. Animals bearing 9L tumors inoculated as described above were anesthetized 15 days following initial 9L-luc tumor inoculation. Briefly, 100 mg/mL ketamine and 10 mg/mL xylazine were added to a mixture of 0.9% normal saline and ethanol at a 10:1 ratio. Rats were given 250 μL ip of ketamine/xylazine solution. A burr hole was made at the same coordinates used for tumor inoculation. A solution of 1:1 PS-COOH and PS-PEG NPs, or PLGA and PLGA-PEG NPs, was co-injected 2.5 mm deep into the brain using a Hamilton syringe and a stereotaxic headframe. Animals were then sacrificed at designated time points of 1 and 24 h following injection. The brain was rapidly removed and placed in OCT on dry ice to slow freeze the tissue to avoid cracking. Tissue was cryosectioned using a Leica 510 cryostat into 12 μm thick slices and stained with DAPI antifade. Slices were imaged in three channels: DAPI for cell nuclei, DS Red for PLGA NPs, and Cy 5 for PLGA-PEG NPs.

Histopathological Analysis of Efficacy Samples. At day 15 after tumor inoculation, brains were harvested standard hematoxylin and eosin (H&E) staining to identify any changes in histological architecture, cell morphology, cellularity, and overall tumor integrity caused by the treatment. One representative animal from each group was sacrificed; the brain was removed and placed in formalin. The tissue was removed from the formalin after 24 h and placed in 70% ethanol solution until paraffin embedding, sectioning, and H&E staining. The tissue sections were examined by a board-certified neuropathologist (C.E.) for evidence of tissue changes, cellular damage, and toxicity.

Conflict of Interest: The authors declare no competing financial interest.

Acknowledgment. The authors thank C. Eberhart for advice on histological analysis of 9L brain tumor tissue. This study was partly funded by the NIH R01 CA164789-02 and NCI U54CA151838. The content is solely the responsibility of the authors and does not necessarily represent the official views of the National Cancer Institute or the National Institutes of Health.

REFERENCES AND NOTES

1. Wen, P. Y.; Kesari, S. Malignant Gliomas in Adults. *N. Engl. J. Med.* **2008**, *359*, 492–507.
2. National Cancer Institute. *CNS and Miscellaneous Intracranial and Intraspinal Neoplasms*; 2010, http://www.cancer.gov/cancertopics/types/brain, accessed October 7, 2014.
3. Preusser, M.; de Ribaupierre, S.; Wohrer, A.; Erridge, S. C.; Hegi, M.; Weller, M.; Stupp, R. Current Concepts and Management of Glioblastoma. *Ann. Neurol.* **2011**, *70*, 9–21.
4. Gruber, M. L.; Hochberg, F. H. Systematic Evaluation of Primary Brain Tumors. *J. Nucl. Med.* **1990**, *31*, 969–971.
5. Stupp, R.; Mason, W. P.; van den Bent, M. J.; Weller, M.; Fisher, B.; Taphoorn, M. J.; Belanger, K.; Brandes, A. A.; Marosi, C.; Bogdahn, U.; *et al.* Radiotherapy Plus Concomitant and Adjuvant Temozolomide for Glioblastoma. *N. Engl. J. Med.* **2005**, *352*, 987–996.
6. Wohlfart, S.; Gelperina, S.; Kreuter, J. Transport of Drugs across the Blood-Brain Barrier by Nanoparticles. *J. Controlled Release* **2012**, *161*, 264–273.
7. Patel, T.; Zhou, J.; Piepmeier, J. M.; Saltzman, W. M. Polymeric Nanoparticles for Drug Delivery to the Central Nervous System. *Adv. Drug Delivery Rev.* **2012**, *64*, 701–705.
8. Fung, L. K.; Shin, M.; Tyler, B.; Brem, H.; Saltzman, W. M. Chemotherapeutic Drugs Released from Polymers: Distribution of 1,3-Bis(2-Chloroethyl)-1-Nitrosourea in the Rat Brain. *Pharm. Res.* **1996**, *13*, 671–682.

9. Allard, E.; Passirani, C.; Benoit, J. P. Convection-Enhanced Delivery of Nanocarriers for the Treatment of Brain Tumors. *Biomaterials* **2009**, *30*, 2302–2318.
10. Degen, J. W.; Walbridge, S.; Vortmeyer, A. O.; Oldfield, E. H.; Lonser, R. R. Safety and Efficacy of Convection-Enhanced Delivery of Gemcitabine or Carboplatin in a Malignant Glioma Model in Rats. *J. Neurosurg.* **2003**, *99*, 893–898.
11. Lopez, K. A.; Waziri, A. E.; Canoll, P. D.; Bruce, J. N. Convection-Enhanced Delivery in the Treatment of Malignant Glioma. *Neurol. Res.* **2006**, *28*, 542–548.
12. Reulen, H. J. Bulk Flow and Diffusion Revisited, and Clinical Applications. *Acta Neurochir. Suppl.* **2010**, *106*, 3–13.
13. Krauze, M. T.; Noble, C. O.; Kawaguchi, T.; Drummond, D.; Kirpotin, D. B.; Yamashita, Y.; Kullberg, E.; Forsayeth, J.; Park, J. W.; Bankiewicz, K. S. Convection-Enhanced Delivery of Nanoliposomal Cpt-11 (Irinotecan) and Pegylated Liposomal Doxorubicin (Doxil) in Rodent Intracranial Brain Tumor Xenografts. *Neuro Oncol.* **2007**, *9*, 393–403.
14. Inoue, T.; Yamashita, Y.; Nishihara, M.; Sugiyama, S.; Sonoda, Y.; Kumabe, T.; Yokoyama, M.; Tominaga, T. Therapeutic Efficacy of a Polymeric Micellar Doxorubicin Infused by Convection-Enhanced Delivery against Intracranial 9l Brain Tumor Models. *Neuro-Oncology* **2009**, *11*, 151–157.
15. Kreuter, J. Nanoparticulate Systems for Brain Delivery of Drugs. *Adv. Drug Delivery Rev.* **2001**, *47*, 65–81.
16. Petri, B.; Bootz, A.; Khalansky, A.; Hekmatara, T.; Muller, R.; Uhl, R.; Kreuter, J.; Gelperina, S. Chemotherapy of Brain Tumour Using Doxorubicin Bound to Surfactant-Coated Poly(butyl cyanoacrylate) Nanoparticles: Revisiting the Role of Surfactants. *J. Controlled Release* **2007**, *117*, 51–58.
17. Steiniger, S. C.; Kreuter, J.; Khalansky, A. S.; Skidan, I. N.; Bobruskin, A. I.; Smirnova, Z. S.; Severin, S. E.; Uhl, R.; Kock, M.; Geiger, K. D.; *et al.* Chemotherapy of Glioblastoma in Rats Using Doxorubicin-Loaded Nanoparticles. *Int. J. Cancer* **2004**, *109*, 759–767.
18. Hekmatara, T.; Bernreuther, C.; Khalansky, A. S.; Theisen, A.; Weissenberger, J.; Matschke, J.; Gelperina, S.; Kreuter, J.; Glatzel, M. Efficient Systemic Therapy of Rat Glioblastoma by Nanoparticle-Bound Doxorubicin Is Due to Antiangiogenic Effects. *Clin. Neuropathol.* **2009**, *28*, 153–164.
19. Nance, E. A.; Woodworth, G. F.; Sailor, K. A.; Shih, T. Y.; Xu, Q.; Swaminathan, G.; Xiang, D.; Eberhart, C.; Hanes, J. A Dense Poly(ethylene glycol) Coating Improves Penetration of Large Polymeric Nanoparticles within Brain Tissue. *Sci. Transl. Med.* **2012**, *4*, 149ra119.
20. Gritsenko, P. G.; Ilina, O.; Friedl, P. Interstitial Guidance of Cancer Invasion. *J. Pathol.* **2012**, *226*, 185–199.
21. Pluen, A.; Boucher, Y.; Ramanujan, S.; McKee, T. D.; Gohongi, T.; di Tomaso, E.; Brown, E. B.; Izumi, Y.; Campbell, R. B.; Berk, D. A.; *et al.* Role of Tumor-Host Interactions in Interstitial Diffusion of Macromolecules: Cranial vs. Subcutaneous Tumors. *Proc. Natl. Acad. Sci. U.S.A.* **2001**, *98*, 4628–4633.
22. Sykova, E.; Nicholson, C. Diffusion in Brain Extracellular Space. *Physiol. Rev.* **2008**, *88*, 1277–1340.
23. Vargova, L.; Homola, A.; Zamecnik, J.; Tichy, M.; Benes, V.; Sykova, E. Diffusion Parameters of the Extracellular Space in Human Gliomas. *Glia* **2003**, *42*, 77–88.
24. Zamecnik, J.; Vargova, L.; Homola, A.; Kodet, R.; Sykova, E. Extracellular Matrix Glycoproteins and Diffusion Barriers in Human Astrocytic Tumours. *Neuropathol. Appl. Neurobiol.* **2004**, *30*, 338–350.
25. Rosso, L.; Brock, C. S.; Gallo, J. M.; Saleem, A.; Price, P. M.; Turkheimer, F. E.; Aboagye, E. O. A New Model for Prediction of Drug Distribution in Tumor and Normal Tissues: Pharmacokinetics of Temozolomide in Glioma Patients. *Cancer Res.* **2009**, *69*, 120–127.
26. Patel, M.; McCully, C.; Godwin, K.; Balis, F. M. Plasma and Cerebrospinal Fluid Pharmacokinetics of Intravenous Temozolomide in Non-Human Primates. *J. Neurooncol.* **2003**, *61*, 203–207.
27. Serwer, L. P.; James, C. D. Challenges in Drug Delivery to Tumors of the Central Nervous System: An Overview of Pharmacological and Surgical Considerations. *Adv. Drug Delivery Rev.* **2012**, *64*, 590–597.
28. Baxter, L. T.; Jain, R. K. Transport of Fluid and Macromolecules in Tumors. I. Role of Interstitial Pressure and Convection. *Microvasc. Res.* **1989**, *37*, 77–104.
29. Baxter, L. T.; Jain, R. K. Transport of Fluid and Macromolecules in Tumors. II. Role of Heterogeneous Perfusion and Lymphatics. *Microvasc. Res.* **1990**, *40*, 246–263.
30. Jain, R. K.; Baxter, L. T. Mechanisms of Heterogeneous Distribution of Monoclonal Antibodies and Other Macromolecules in Tumors: Significance of Elevated Interstitial Pressure. *Cancer Res.* **1988**, *48*, 7022–7032.
31. Boucher, Y.; Baxter, L. T.; Jain, R. K. Interstitial Pressure Gradients in Tissue-Isolated and Subcutaneous Tumors: Implications for Therapy. *Cancer Res.* **1990**, *50*, 4478–4484.
32. Bhalla, K. N. Microtubule-Targeted Anticancer Agents and Apoptosis. *Oncogene* **2003**, *22*, 9075–9086.
33. Zhou, J.; Patel, T. R.; Sirianni, R. W.; Strohbehn, G.; Zheng, M. Q.; Duong, N.; Schafbauer, T.; Huttner, A. J.; Huang, Y.; Carson, R. E.; *et al.* Highly Penetrative, Drug-Loaded Nanocarriers Improve Treatment of Glioblastoma. *Proc. Natl. Acad. Sci. U.S.A.* **2013**, *110*, 11751–11756.
34. Wohlfart, S.; Khalansky, A. S.; Gelperina, S.; Maksimenko, O.; Bernreuther, C.; Glatzel, M.; Kreuter, J. Efficient Chemotherapy of Rat Glioblastoma Using Doxorubicin-Loaded Plga Nanoparticles with Different Stabilizers. *PLoS One* **2011**, *6*, e19121.
35. Gelperina, S.; Maksimenko, O.; Khalansky, A.; Vanchugova, L.; Shipulo, E.; Abbasova, K.; Berdiev, R.; Wohlfart, S.; Chepurnova, N.; Kreuter, J. Drug Delivery to the Brain Using Surfactant-Coated Poly(lactide-co-glycolide) Nanoparticles: Influence of the Formulation Parameters. *Eur. J. Pharm. Biopharm.* **2010**, *74*, 157–163.
36. Zensi, A.; Begley, D.; Pontikis, C.; Legros, C.; Mihoreanu, L.; Buchel, C.; Kreuter, J. Human Serum Albumin Nanoparticles Modified with Apolipoprotein a-I Cross the Blood-Brain Barrier and Enter the Rodent Brain. *J. Drug Target* **2010**, *18*, 842–848.
37. Zensi, A.; Begley, D.; Pontikis, C.; Legros, C.; Mihoreanu, L.; Wagner, S.; Buchel, C.; von Briesen, H.; Kreuter, J. Albumin Nanoparticles Targeted with Apo E Enter the Cns by Transcytosis and Are Delivered to Neurones. *J. Controlled Release* **2009**, *137*, 78–86.
38. Amoozgar, Z.; Yeo, Y. Recent Advances in Stealth Coating of Nanoparticle Drug Delivery Systems. *Wiley Interdiscip Rev. Nanomed. Nanobiotechnol.* **2012**, *4*, 219–233.
39. Gref, R.; Minamitake, Y.; Peracchia, M. T.; Trubetskoy, V.; Torchilin, V.; Langer, R. Biodegradable Long-Circulating Polymeric Nanospheres. *Science* **1994**, *263*, 1600–1603.
40. Maruyama, K. Intracellular Targeting Delivery of Liposomal Drugs to Solid Tumors Based on EPR Effects. *Adv. Drug Delivery Rev.* **2011**, *63*, 161–169.
41. Claes, A.; Idema, A. J.; Wesseling, P. Diffuse Glioma Growth: A Guerilla War. *Acta Neuropathol.* **2007**, *114*, 443–458.
42. Treat, L. H.; McDannold, N.; Zhang, Y.; Vykhodtseva, N.; Hynynen, K. Improved Anti-Tumor Effect of Liposomal Doxorubicin after Targeted Blood-Brain Barrier Disruption by MRI-Guided Focused Ultrasound in Rat Glioma. *Ultrasound Med. Biol.* **2012**, *38*, 1716–1725.
43. Yang, F. Y.; Lin, G. L.; Horng, S. C.; Chang, T. K.; Wu, S. Y.; Wong, T. T.; Wang, H. E. Pulsed High-Intensity Focused Ultrasound Enhances the Relative Permeability of the Blood-Tumor Barrier in a Glioma-Bearing Rat Model. *IEEE Trans Ultrason. Ferroelectr. Freq. Control* **2011**, *58*, 964–970.
44. Liu, H. L.; Hua, M. Y.; Chen, P. Y.; Chu, P. C.; Pan, C. H.; Yang, H. W.; Huang, C. Y.; Wang, J. J.; Yen, T. C.; Wei, K. C. Blood-Brain Barrier Disruption with Focused Ultrasound Enhances Delivery of Chemotherapeutic Drugs for Glioblastoma Treatment. *Radiology* **2010**, *255*, 415–425.
45. Nance, E. A.; Timbie, K.; Miller, G. W.; Song, J.; Louttit, C.; Klibanov, A. L.; Shih, T.-S.; Swamination, G.; Tamargo, R. J.; Woodworth, G. F.; Hanes, J.; Price, R. Noninvasive Delivery of Stealth, Brain-Penetrating Nanoparticles across the Blood-Brain Barrier Using Mri-Guided Focused Ultrasound. *J. Controlled Release* **2014**in press.
46. McDannold, N.; Arvanitis, C. D.; Vykhodtseva, N.; Livingstone, M. S. Temporary Disruption of the Blood-Brain

Barrier by Use of Ultrasound and Microbubbles: Safety and Efficacy Evaluation in Rhesus Macaques. *Cancer Res.* **2012**, *72*, 3652–3663.
47. Kinoshita, M.; McDannold, N.; Jolesz, F. A.; Hynynen, K. Noninvasive Localized Delivery of Herceptin to the Mouse Brain by MRI-Guided Focused Ultrasound-Induced Blood-Brain Barrier Disruption. *Proc. Natl. Acad. Sci. U.S.A.* **2006**, *103*, 11719–11723.
48. Jordao, J. F.; Ayala-Grosso, C. A.; Markham, K.; Huang, Y.; Chopra, R.; McLaurin, J.; Hynynen, K.; Aubert, I. Antibodies Targeted to the Brain with Image-Guided Focused Ultrasound Reduces Amyloid-Beta Plaque Load in the Tgcrnd8Mouse Model of Alzheimer's Disease. *PLoS One* **2010**, *5*, e10549.
49. Yoo, H. S.; Oh, J. E.; Lee, K. H.; Park, T. G. Biodegradable Nanoparticles Containing Doxorubicin-Plga Conjugate for Sustained Release. *Pharm. Res.* **1999**, *16*, 1114–1118.
50. Xu, Q.; Boylan, N. J.; Cai, S.; Miao, B.; Patel, H.; Hanes, J. Scalable Method to Produce Biodegradable Nanoparticles That Rapidly Penetrate Human Mucus. *J. Controlled Release* **2013**, *170*, 279–286.
51. Lai, S. K.; O'Hanlon, D. E.; Harrold, S.; Man, S. T.; Wang, Y. Y.; Cone, R.; Hanes, J. Rapid Transport of Large Polymeric Nanoparticles in Fresh Undiluted Human Mucus. *Proc. Natl. Acad. Sci. U.S.A.* **2007**, *104*, 1482–1487.
52. Crocker, J. C.; Grier, D. G. Methods of Digital Video Microscopy for Colloidal Surfaces. *J. Colloid Interface Sci.* **1996**, *179*, 298–310.
53. Schuster, B. S.; Kim, A. J.; Kays, J. C.; Kanzawa, M. M.; Guggino, W. B.; Boyle, M. P.; Rowe, S. M.; Muzyczka, N.; Suk, J. S.; Hanes, J. Overcoming the Cystic Fibrosis Sputum Barrier to Leading Adeno-Associated Virus Gene Therapy Vectors. *Mol. Ther.* **2014**, *22*, 1484–1493.
54. Suh, J.; Dawson, M.; Hanes, J. Real-Time Multiple-Particle Tracking: Applications to Drug and Gene Delivery. *Adv. Drug Delivery Rev.* **2005**, *57*, 63–78.
55. Gullotti, E.; Yeo, Y. Beyond the Imaging: Limitations of Cellular Uptake Study in the Evaluation of Nanoparticles. *J. Controlled Release* **2012**, *164*, 170–176.